Materials Science in Semiconductor Processing 96 (2019) 1–7

Contents lists available at ScienceDirect

Materials Science in Semiconductor Processing

journal homepage: www.elsevier.com/locate/mssp

Ultra-thin stack of n-type hydrogenated microcrystalline silicon and silicon oxide front contact layer for rear-emitter silicon heterojunction solar cells

Duy Phong Pham[a], Sangho Kim[b], Sehyeon Kim[a], Sunhwa Lee[a], Anh Huy Tuan Le[c,d], Jinjoo Park[a,*], Junsin Yi[a,*]

[a] College of Information and Communication Engineering, Sungkyunkwan University, 2066 Seobu-ro, Suwon-si, Gyeonggi-do 16419, South Korea
[b] Department of Energy Science, Sungkyunkwan University, 2066 Seobu-ro, Suwon-si, Gyeonggi-do 16419, South Korea
[c] Division of Computational Physics, Institute for Computational Science, Ton Duc Thang University, Ho Chi Minh City, Vietnam
[d] Faculty of Electrical and Electronics Engineering, Ton Duc Thang University, Ho Chi Minh City, Vietnam

ARTICLE INFO

Keywords:
Rear-emitter silicon heterojunction solar cells
Hydrogenated microcrystalline silicon oxide films
Front contact layers

ABSTRACT

We demonstrate the clear advantage of a n-type hydrogenated microcrystalline silicon (n-μc-Si:H) seed layer on the optoelectronic properties and crystallisation behaviour of n-type hydrogenated microcrystalline silicon oxide (n-μc-SiO_x:H) front contact layers. The presence of a non-oxidic n-μc-Si:H seed layer can reduce the thickness and refractive index of the n-μc-SiO_x:H front layer significantly while maintaining a high degree of crystallisation and excellent conductivity. This leads to increase in short-circuit current density (J_{sc}) by 2.64% and open-circuit voltage (V_{oc}) by 0.56% in comparison to that of a device without the seed layer. The enhancement in J_{sc} can be attributed to the reduction in parasitic absorption loss in the extremely thin front layer. In addition, the improvement in V_{oc} can result from enhanced surface passivation of the wafer due to seed layer growth in very high hydrogen plasma environment which can play a role as the hydrogen post-plasma treatment. The low thickness of the n-μc-SiO_x:H front layer yields lower internal recombination losses. In conjunction with an optimised n-μc-Si:H seed layer and n-μc-SiO_x:H front layer, we obtained a high conversion efficiency value of 21.8% with V_{oc} of 727 mV, J_{sc} of 39 mA/cm^2, and FF of 77% among the fabricated cells in laboratory.

1. Introduction

Silicon heterojunction (SHJ) solar cells owe their progress in performance to excellent passivation effects on both sides of the crystalline silicon wafer surface. SHJ solar cells have been in the research forefront for more than twenty years due to the following advantages: a) simple and cost-effective production process without the need for patterning steps, b) high open-circuit voltage (V_{oc}) in comparison with the traditional homojunction crystalline silicon cells, and c) good performance stability [1,2]. High efficiencies far over 24% have been reported for the SHJ cell until now [3–5]. Numerous efforts have been made to improve the SHJ solar cells further by focusing on the following aspects: 1) reducing carrier recombination loss by high-quality surface passivation layer [6,7]; 2) reducing parasitic absorption loss at the front side by optimising the front grid silver electrode with higher aspect ratio and conductivity and/or developing ultra-thin wide-gap front contact layers; and, 3) reducing the material cost and carrier collection loss by using thinner wafers [8,9]. Among these, losses due to optical parasitic absorption at the front contact layer pose an enormous challenge which limits the performance of SHJ solar cells [10,11].

Generally, in the front junction configuration, p-type doped layers are situated on the front side to collect those minority charge carriers that are generated close to their collecting contact in an efficient manner. This is really necessary in the case of short-lifetime absorber materials with small carrier diffusion lengths of minority charge carriers [1,12]. However, with good surface passivation of hydrogenated amorphous silicon (a-Si:H) materials as also high-quality absorber wafers available today, the use of a p-type front contact layer in SHJ solar cells is less demanding as the minority charge carriers can diffuse effectively to their collecting electrode regardless of the location of the electrode [13]. In addition, a Schottky barrier is formed between the p-type front contact and transparent conducting oxide (TCO) layers due to the inherent weak conductivity of the front surface field layer [14,15]. A thick and/or highly doped p-layer, formed at the expense of optical transparency, is normally able to eliminate this barrier and thus forming a suitable front surface field for hole collection. However, this results in parasitic absorption and carrier recombination at the junction which adversely affects the solar cell parameters, V_{oc}, fill factor (FF),

* Corresponding authors.
E-mail addresses: pdphong@skku.edu (D.P. Pham), lehuytuananh@tdtu.edu.vn (A.H.T. Le), jwjh3516@skku.edu (J. Park), junsin@skku.edu (J. Yi).

https://doi.org/10.1016/j.mssp.2019.02.017
Received 22 October 2018; Received in revised form 28 January 2019; Accepted 15 February 2019
Available online 20 February 2019
1369-8001/

and short-circuit current density (J_{sc}). It appears that the contact formation for hole collection at the front side is a delicate task [16]. Efforts made in this direction saw the evolution of a new SHJ device architecture, in which the p-contact layer is located on the rear side, popularly known as the rear-emitter silicon heterojunction (RE-SHJ) solar cell [17,18].

In RE-SHJ configuration, a thicker and/or highly conducting p-contact layer can be used at rear side regardless of any major transparency concerns. The use of the RE-SHJ design relaxes the strict requirement of the front TCO material and, at the same time, avails more optical transmission into the bulk absorber (wafer) through a very thin, n-type front layer without seriously impairing conductivity [13,19]. Standard RE-SHJ solar cells use n- and p-doped hydrogenated amorphous silicon (n-a-Si:H and p-a-Si:H) as carrier-selective front and back contact layers, respectively [20]. The efficient internal electric field which helps to separate and collect carrier charges depends strongly on the net doping of these doped layers. However, a highly uniform degree of doping is hardly ever achieved with a-Si:H material because large dopant quantities cause accumulation of defect density. This has a detrimental effect on uniform doping and even likely to deteriorate the passivation quality at wafer interfaces [21]. Additionally, the low bandgap of the a-Si:H material hinders the transparency of the solar spectrum in the short wavelength region. A material with wide bandgap and high conductivity appears most suitable to alleviate this problem.

Hydrogenated microcrystalline silicon (μc-Si:H) is found to be highly attractive as a front contact layer in thin film silicon solar cells [22,23] as well as SHJ solar cells [24,25]; this is owing to its high doping efficiency thanks to a crystalline phase and low absorption coefficient in the short wavelength region in comparison to the a-Si:H counterpart. By incorporating oxygen, a bi-phase microcrystalline silicon oxide (μc-SiO_x:H) material with columnar crystalline silicon phase mixed in an amorphous silicon oxide matrix phase and considerably improved transparency can be obtained without significantly affecting vertical conductivity [13,24,26]. In such a bi-phase material, high vertical conductivity is achieved throughout crystalline phase while the amorphous oxide phase is responsible for enhanced transparency. A challenge in realising μc-SiO_x:H as the front contact layer in SHJ solar cells is the formation of ultra-thin layers with high-crystalline quality and efficient doping without impairing the a-Si:H passivation layers below. It requires delicate control of the initial nucleation processes to limit the incubation phase during crystal growth of n-μc-SiO_x:H layer.

In this work, we investigate a stack of front contact layers for RE-SHJ solar cells including a very thin n-μc-Si:H layer grown under high hydrogen dilution and at low plasma power density in a favourable nucleation environment for subsequent growth of n-μc-SiO_x:H layers. This study helped us to evaluate the optimum thickness of n-μc-SiO_x:H layers that are endowed with high crystalline fraction and electrical conductivity. The analysis of solar cell parameters, namely short-circuit current density (J_{sc}) in the short wavelength region, open-circuit voltage (V_{oc}), and fill factor (FF) based on a stack of seed-crystalline layer and ultra-thin n-μc-SiO_x:H front layer is presented.

2. Experiment

Single layers of n-μc-SiO_x:H with various thicknesses were deposited on EAGLE XG™ glass substrates using a cluster multi-chamber plasma enhanced chemical vapor deposition (PECVD) system. To fast prompt nucleation for n-μc-SiO_x:H growth, the substrate was firstly deposited with n-μc-Si:H (seed layer) of 3 nm thickness in the gas mixture consisting of silane (SiH_4), hydrogen (H_2), and phosphine (PH_3). After the n-μc-Si:H deposition, the plasma discharge power was interrupted. Then, the second gas mixture including of SiH_4, H_2, PH_3 and carbon dioxide (CO_2) was set up for subsequent n-μc-SiO_x:H growth. The deposition parameters of these layers are summarized in Table 1. Optical properties including absorption coefficient (α), and reflective index (n) of n-μc-SiO_x:H layers with and without the seed layer were extracted by fitting spectroscopic ellipsometry (SE - VASE® Ellipsometer - J. A. Woollam Co., Inc.) data using Tauc-Lorentz model in the wavelength range from 240 to 1700 nm at incident angle of 65°. The lateral conductivity of these samples was measured using evaporated aluminium coplanar bi-electrodes (250-μm spacing) with a programmable Keithley 617 electrometer. Structural characteristics were evaluated by Raman spectroscopy (Ramboss 500i, Dongwoo Optron Co., Ltd.).

Table 1
Deposition parameters of n-μc-Si:H seed layer and n-μc-SiO_x:H front layers.

Deposition Condition	n-μc-Si:H	n-μc-SiO_x:H
$[H_2]/[SiH_4]$ gas flux ratio	160	125
$[PH_3]/[SiH_4]$ gas flux ratio	0.6	2
$[CO_2]/[SiH_4]$ gas flux ratio	0	0.5
Power density (mW/cm^2)	42	42
Working Pressure (Torr)	1.5	1.5
Deposition temperature (°C)	110	110
Thickness (nm)	3	**4–17**

The RE-SHJ solar cells were fabricated on random pyramid structure obtained on a textured n-type Czochralski wafer of 140 μm thickness and 4.3 Ω cm resistivity as shown in the schematic diagram in Fig. 1. The cell area was calibrated by indium-doped tin oxide (ITO) membrane deposited using a mask area of 10.24 cm^2. After screen printing a Ag-grid electrode on the front side and Ag back electrode using commercial paste (KYOTO) at 160 °C, the fabricated solar cells were characterised by I–V curves in dark and illuminated conditions measured under standard test conditions (one-sun illumination, 25 °C, AM1.5 spectrum, 100 mW/cm^2 incident light power) through 10.24 cm^2 shadow mask. The width and height of the front Ag-grid electrode were optimised as 40 μm and 20 μm, respectively, to reduce the shadowing down to ~ 4%. In addition, the external quantum efficiency (EQE) was measured using a solar cell quantum efficiency measurement system (QEX7, PV Measurement Inc.) in the wavelength range of 300–1100 nm.

3. Result and discussion

First, we estimated the optoelectronic and structural characteristics of single n-μc-SiO_x:H layers of various thicknesses deposited in the following geometry: glass substrate/seed layer of 3 nm/n-μc-SiO_x:H layer (varies from 5 to 17 nm). The characteristics of single n-μc-SiO_x:H layers without the seed layer were derived for comparison. The optoelectronic properties of these samples, such as the lateral conductivity (σ) and refractive index (n) at 400 and 632 nm are shown in Table 2. Fig. 2 shows plots of $\{\alpha(E)E\}^{1/2}$ versus photon energy E as used for the determination of optical band-gap of the films. It shows that all n-μc-SiO_x:H films have a wide optical band gap around 2.1–2.4 eV. The structural analyses of such layers using Raman spectroscopy are shown in Fig. 3a and b. Crystalline volume factor (X_c) as shown in Fig. 3c was derived from the data using the relation $X_c = I_{518} / (I_{518} + I_{480})$, in which I_{518} and I_{480} are the integrated areas extracted from Gaussian fitting at 518 and 480 cm^{-1}, respectively. We can see in Fig. 3a that the n-μc-SiO_x layer structure without a bottom-seed-layer appears to present a clear crystalline phase, which is characterised by a sharp Raman peak at 518 cm^{-1}, mainly visible at thicknesses above the value of 17 nm. On the contrary, for thicknesses in the range of 5–13 nm, the structure can be regarded essentially as an amorphous phase, as defined by a broad spectral range centered around 480 cm^{-1}. It has been known that the growth of crystalline phase in silicon films during plasma deposition is generally initiated through a first incubation amorphous phase followed by nucleation and, finally, crystalline phase formation [27–29]. In this process, nucleation-growth aggregation plays an important role to prompt subsequent crystalline particles. As shown in Fig. 3b, the crystalline phase of n-μc-SiO_x layer can be initiated even at a low thickness of 7 nm in conjunction with a previously

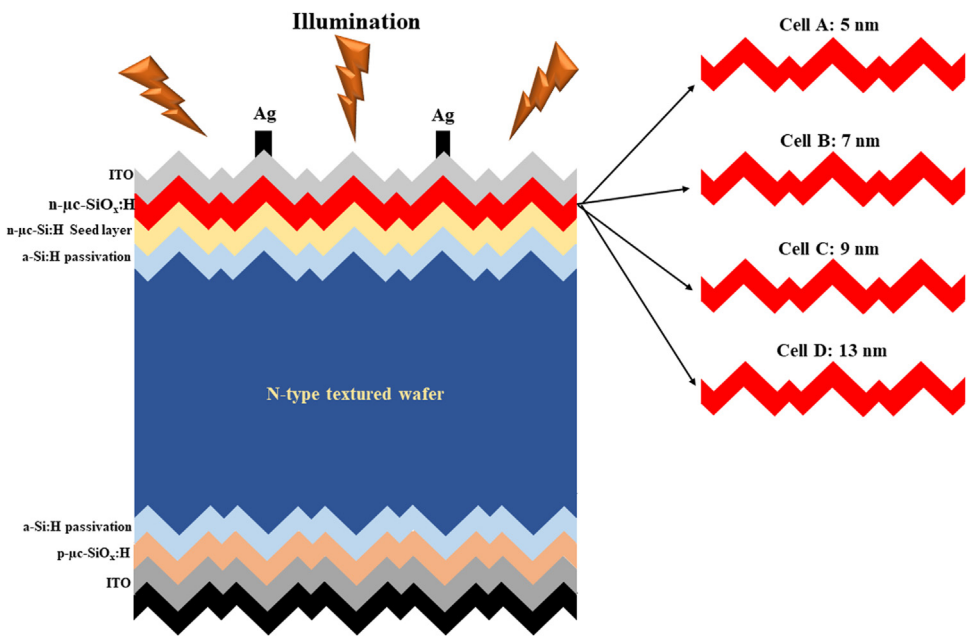

Fig. 1. Schematic diagram RE-SHJ solar cell structure with various thickness of n-μc-SiO_x:H front contact layers.

prepared seed layer. Table 1 lists the deposition parameters of the seed layer prepared in very high $[H_2]/[SiH_4]$ gas ratio of 160. It has been reported by many research groups that the seed layer formed at very high $[H_2]/[SiH_4]$ gas ratios (~160, without added CO_2 gas content) has a hydrogenated silicon structure with micro or nano-crystallite particles including vertical columnar-crystalline phases enveloped by amorphous phase at the boundaries [27,30–32]. Here, because of the seed layer thickness of approximately 3 nm, a crystalline-nucleation behaviour is observed for subsequent layer growth. The seed layer plays a significant role in prompting the rapid growth of crystalline phase in the n-μc-SiO_x layer even with a low thickness of 7 nm. Based on the nucleation kinetics, the crystalline phase may grow rapidly and increase in thickness [28]. This is discernible in Fig. 3c where the value of X_c increases with thickness of n-μc-SiO_x:H layer.

The crystalline phase formation is considerably meaningful when high conductivity of bi-phase front n-μc-SiO_x material is regarded. As seen in Table 2, the conductivity of the 7-nm thick n-μc-SiO_x-seed layer stack is four orders of magnitude higher than that of the film without the seed layer. The conductivity is seen to increase with thickness. From the behaviour of X_c in Fig. 3c, it infers that the conductivity appears to rise with increase in the crystalline volume factor (X_c). In addition, the sooner crystalline phase formation of films at 7–9 nm thickness with seed layer is also significant meaningful to reducing the thickness of n-μc-SiO_x front layer, i.e. high transparency and/or low parasitic absorption. We can see that while the conductivity is nearly analogous with 17 nm film without seed layer, the refractive index at 400 nm and 632 nm wavelength of 7–9 nm-film with seed layer is significantly lower. This means that by maintaining the high conductivity for effective carrier collection to obtain high V_{oc} and FF, the thin n-μc-SiO_x front layer (thickness of 7–9 nm) together with the seed layer can significantly lower parasitic absorption losses; this yields higher values of J_{sc} than that in the case of using thicker (greater than 17 nm) n-μc-SiO_x front layers.

To validate the observed properties, several RE-SHJ solar cells with different n-μc-SiO_x front layer thicknesses were fabricated on 3-nm thick seed layers in a configuration shown in Fig. 1. A RE-SHJ reference cell (cell E) with 17-nm thick n-μc-SiO_x front layer but without the seed layer was also prepared for control data. The cell parameters, namely V_{oc}, J_{sc}, FF, and efficiency (E_{ff}) of all the cells fabricated are summarized in Table 3 and J-V curves under one-sun illumination were plotted in Fig. 4a. We can see that the lowest V_{oc} and FF values are attributed to a cell (A) which is probably due to incomplete crystallisation of thin n-μc-SiO_x front layer of 5 nm as indicated in Fig. 3b. With completely formed crystalline phase on the seed layer of the n-μc-SiO_x front layer, the V_{oc} and FF of the cells (from B to D) are considerably higher than those of cell A. It is notable that with the seed layer on cells B, C, and D, the parameters V_{oc} and J_{sc} have significantly improved in comparison with those of the reference cell (E). The higher values of J_{sc} are attributed to the drastically reduced thickness of the front layer, which can result in significantly lower losses due to parasitic absorption and internal recombination. The former is discernible in the EQE characteristics as shown in Fig. 4b. The EQE of the cell with the seed layer is considerably higher than that of the reference cell, especially in short wavelength region of 300–600 nm.

Table 2
Conductivity and refractive index of n-μc-SiO_x:H with various thickness deposited with and without seed layer.

Thickness (nm)	With seed layer			Without seed layer		
	Conductivity (S/cm)	Refractive index at		Conductivity (S/cm)	Refractive index at	
		400 nm	632 nm		400 nm	632 nm
5	2.0×10^{-6}	3.42	2.76	1.0×10^{-6}	2.70	2.34
7	1.5×10^{-2}	3.45	2.79	3.0×10^{-6}	2.83	2.40
9	7.2×10^{-2}	3.48	2.81	9.0×10^{-6}	2.95	2.48
13	1.2×10^{-1}	3.70	2.91	2.1×10^{-4}	3.30	2.7
17	9.0×10^{-1}	3.72	3.0	8.0×10^{-2}	3.55	2.85

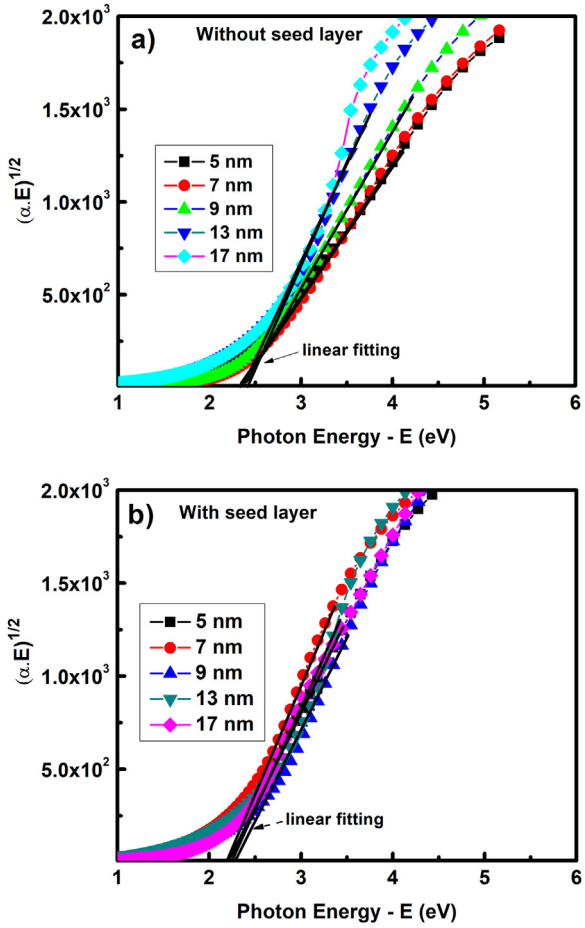

Fig. 2. Plots of $\{\alpha(E)E\}^{1/2}$ versus photon energy E from which the optical band gap is extracted by the linear fitting.

The observed high V_{oc} of the cells B, C and D can be understood from the contribution of the n-μc-Si:H seed layer. Mazzarella et al. reported that the surface passivation quality of the wafer improves during growth of subsequent n-μc-Si:H layer in very high hydrogen dilution [33]. This is akin to the post-hydrogen plasma treatment which is often applied to a very thin a-Si:H layer to passivate dangling bonds on the wafer surface. To understand the mechanism better, we measured the minority carrier lifetime in all cell precursor components prior to ITO deposition, i.e. after p- and n-layer deposition as shown in Fig. 5a. Measured values were compared with that of wafer prior to n-layer deposition (reference wafer - RW) as shown in Fig. 5b. In addition, Fig. 5c summarizes the lifetime and implied V_{oc} (i-V_{oc}) values at one-sun illumination of the components as depicted in Fig. 5a. Fig. 5c shows that the lifetime and i-V_{oc} of the reference cell (E) were insignificantly higher compared with that of RW while that of the cells (B – D) were considerably enhanced compared with that of RW. This indicates that the seed μc-Si:H layer played essentially role in not only promoting fast the crystalline-growth of subsequent μc-SiO_x:H layer but also enhancing passivation quality of wafer surface. As a results, the V_{oc} of cells B-D was considerably higher than that of cell E, as shown in Table 3. A lower lifetime and i-V_{oc} of cell A compared with that of cell E is probable to the uncompleted crystallisation of thin n-μc-SiO_x front layer which can cause more defects in film structure and thus deteriorate the V_{oc} and FF, as shown in Table 3. It can be concluded that if the crystalline-growth is enhanced by the seed layer, the subsequent n-μc-SiO_x:H layer can gain a sufficient conductivity even at a thin thickness to reduce the parasitic absorption losses. In addition, complete crystalline-growth of n-μc-SiO_x front layer on the seed layer can enhance the passivation quality of wafer surface and thus result in high V_{oc} and FF.

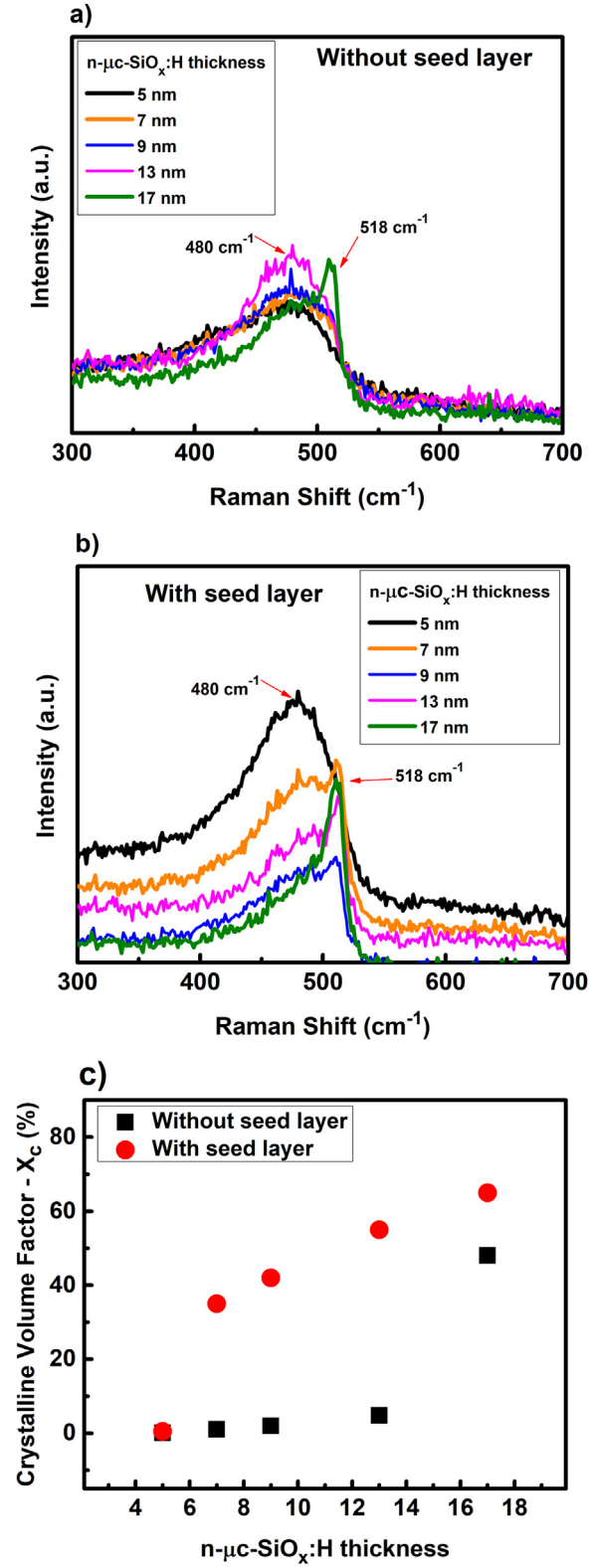

Fig. 3. Raman spectra of n-μc-SiO_x:H front contact layers: a) without and b) with the seed layer; and c) the crystalline volume factors (X_c) of n-μc-SiO_x:H front contact layers with and without the seed layer as a function of thickness.

Basically, a solar cell is attributed to be a diode. In the dark, characteristic of a solar cell behaves completely like a diode. We measured and analyzed the dark I–V (DIV) characteristic on each of the cells based on the diffusion model of the single diode, to obtain better insight

Table 3
The cell parameters including V_{oc}, J_{sc}, FF and Efficiency of SHJ solar cells.

RE-SHJ solar cells	Seed layer thickness (nm)	n-μc-SiO_x:H thickness (nm)	V_{oc} (mV)	J_{sc} (mA/cm^2)	FF (%)	Efficiency (%)
A	3	5	717	38.3	70	19.2
B	3	7	725	39	75	21.2
C	3	9	727	39	77	21.8
D	3	13	726	38.5	75	21
E	0	17	723	38	76	20.8

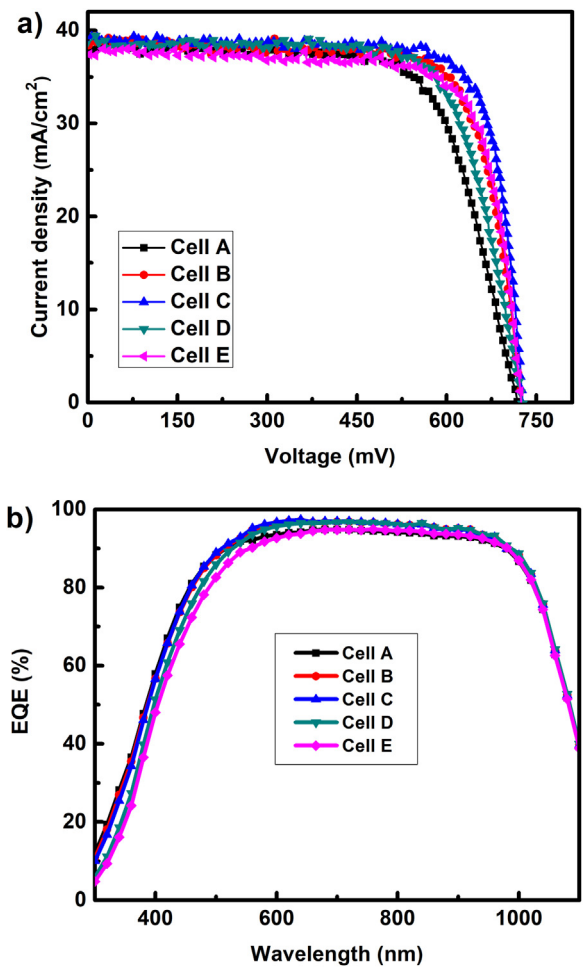

Fig. 4. a) J-V curves under one-sun illumination and b) external quantum efficiencies of RE-SHJ solar cells.

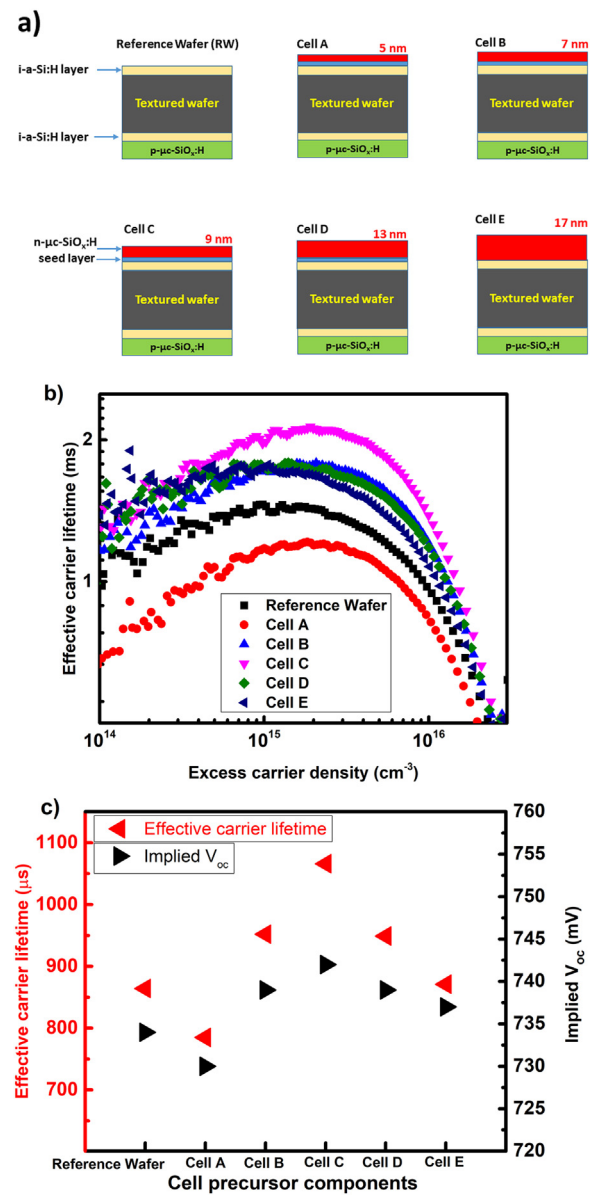

Fig. 5. a) Schematic diagram of all cell precursor components for the minority carrier lifetime measurement; b) effective carrier lifetime of these precursor components as a function of excess carrier density; and c) effective carrier lifetime and implied V_{oc} values at one-sun illumination as a function of cell precursor components.

into the enhanced quality of the cells. From DIV characteristics, the diode ideal factor (n_o) and inverse saturation current density (J_o) were extracted as shown in Fig. 6a and b [34] and summarized in Fig. 6c. For crystalline silicon solar cells, n_o towards 1 means that the diffusion current can be preponderant. In case of n_o towards a value far higher than 1, this means that the generation/recombination current dominates. Cell A gives the highest values of n_o and J_o as shown in Fig. 6c. A higher value of n reflects when the recombination current dominates the diode conduction mechanism [35,36]. It is now clearly evident that cell A is beset with defects caused by incomplete crystallisation. With improved crystallisation and thinner front layers of n-μc-SiO_x, cells B and D display much lower n_o and J_o values than that of the reference cell (E) thus reinforcing the critical role of the seed layer in reducing internal recombination losses in the n-μc-SiO_x front layer and to realise high values of V_{oc}.

In conclusion, doped wide-gap μc-SiO_x:H materials have been used successfully as front contact layer in SHJ solar cells [25,33,37]. The challenge is still to grow very thin and highly crystalline films to reduce significantly the parasitic absorption while maintaining the effective carrier collection. Here, we indicated that the n-μc-SiO_x:H front layer grown on the n-μc-Si:H seed layer can gain highly crystalline with considerably thinner thickness than the n-μc-SiO_x:H without seed layer. It has been indicated that introducing oxygen into μc-Si:H network restricts the crystalline-growth because numerous Si will bond to

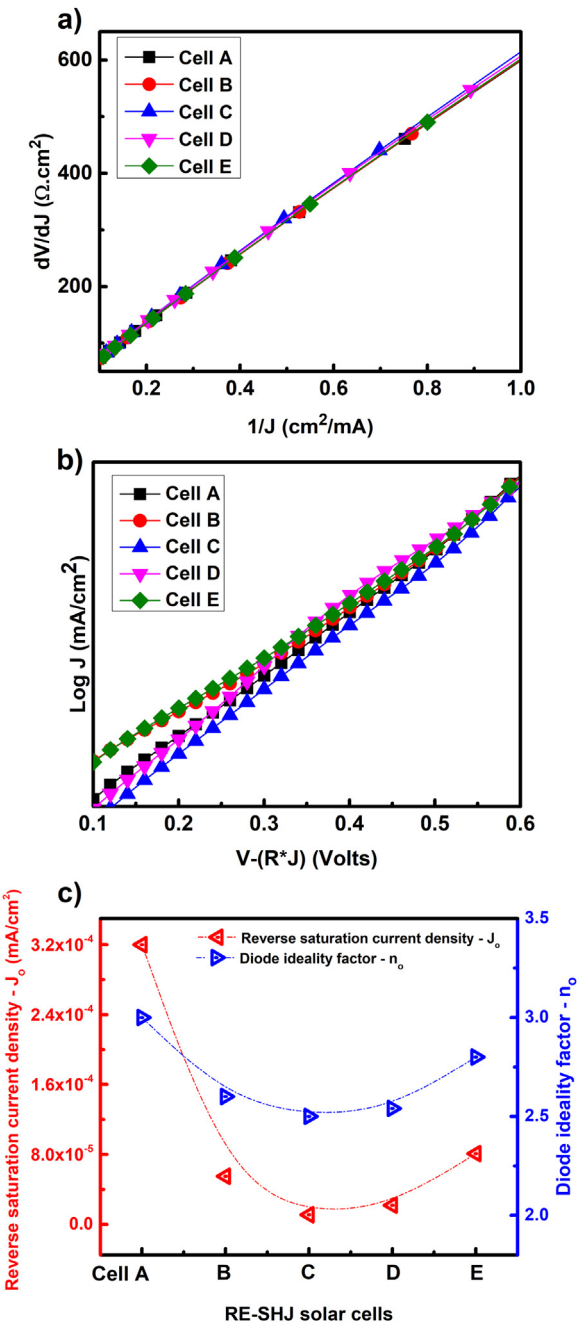

Fig. 6. a) Plot of dV/dJ as a function of 1/J for all RE-SHJ solar cells (the intercepts of linear fittings are series resistances (R_s)); b) Plot of logJ as a function of (V-JR) (the slopes of linear fittings give q/n_okT ratios and intercepts are J_o values); and c) n_o and J_o values of all RE-SHJ solar cells.

oxygen into Si-O-Si form, and thus diminishing the possible number of available Si to form Si-Si bonding in nano-crystallites [26,37,38]. In addition, μc-Si:H film quality deteriorates with incorporating oxygen [39]. Consequently, it will be better if using a μc-Si:H materials as an initial seed layer for subsequent crystalline-growth of n-μc-SiO_x:H layer.

4. Conclusion

We have investigated the optoelectronic properties and structure of n-μc-SiO_x front contact layers of various thicknesses grown on n-μc-Si:H seed layer for RE-SHJ solar cells. At a threshold thickness, the stack (film with a seed layer) shows excellent optoelectronic properties with low refractive index (i.e. high transparency) while maintaining a high fraction of crystalline phase and high electrical conductivity in comparison to films without the seed layer. In application to RE-SHJ solar cells, the lower refractive index yields J_{sc} improvement by 2.64% which is attributed to reduced parasitic absorption loss by virtue of the low thickness of the front contact layer. The enhancement of 0.56% in V_{oc} is due to improved surface passivation under specific conditions of PECVD growth of the seed layer in very high hydrogen dilution which play a critical role during post-hydrogen plasma treatment. An extremely low thickness of the n-μc-SiO_x front contact layer facilitates reduced internal recombination loss. With optimised seed and front contact layer thickness, the best fabricated RE-SHJ solar cell shows a high efficiency value of 21.8%.

Acknowledgments

This work was supported by the New & Renewable Energy Core Technology Program of the Korea Institute of Energy Technology Evaluation and Planning (KETEP), granted financial resource from the Ministry of Trade, Industry & Energy, Republic of Korea (No. 20163010012230). This work was also supported by the Korea Institute Technology Evaluation and Planning funded by the Ministry of Trade, Industry & Energy of the Republic of Korea (20173010012940).

References

[1] S. De Wolf, A. Descoeudres, Z.C. Holman, C. Ballif, High-efficiency silicon heterojunction solar cells: a Review, Green 2 (1) (2012).
[2] J. Liu, Y. Yao, S. Xiao, X. Gu, Review of status developments of high-efficiency crystalline silicon solar cells, J. Phys. D Appl. Phys. 51 (12) (2018) 123001.
[3] K. Masuko, M. Shigematsu, T. Hashiguchi, D. Fujishima, M. Kai, N. Yoshimura, T. Yamaguchi, Y. Ichihashi, T. Mishima, N. Matsubara, T. Yamanishi, T. Takahama, M. Taguchi, E. Maruyama, S. Okamoto, Achievement of more than 25% conversion efficiency with crystalline silicon heterojunction solar cell, IEEE J. Photovolt. 4 (6) (2014) 1433.
[4] M. Taguchi, A. Yano, S. Tohoda, K. Matsuyama, Y. Nakamura, T. Nishiwaki, K. Fujita, E. Maruyama, IEEE J. Photovolt. 4 (1) (2014) 96.
[5] D. Adachi, J.L. Hernández, K. Yamamoto, Impact of carrier recombination on fill factor for large area heterojunction crystalline silicon solar cell with 25.1% efficiency, Appl. Phys. Lett. 107 (23) (2015) 233506.
[6] M. Taguchi, K. Kawamoto, S. Tsuge, T. Baba, H. Sakata, M. Morizane, K. Uchihashi, N. Nakamura, S. Kiyama, O. Oota, Prog. Photovolt. Res. Appl. 8 (2000) 503–513.
[7] M. Taguchi, A. Terakawa, E. Maruyama, M. Tanaka, Obtaining a higher Voc in HIT cells, Prog. Photovolt. Res. Appl. 13 (6) (2005) 481–488.
[8] K. Maki, D. Fujishima, H. Inoue, Y. Tsunomura, T. Asaumi, S. Taira, T. Kinoshita, M. Taguchi, H. Sakata, H. Kanno, E. Maruyama, High-efficiency HIT solar cells with a very thin structure enabling a high V_{oc}, IEEE 37th Photovoltaic Specialists Conference (PVSC) (2011) 000057-000061.
[9] T. Kinoshita, D. Fujishima, A. Yano, A. Ogane, S. Tohoda, K. Matsuyama, Y. Nakamura, N. Tokuoka, H. Kanno, H. Sakata, M. Taguchi, E. Maruyama, The approaches for high efficiency HIT^{TM} solar cell with very thin (< 100 μm) silicon wafer over 23%, Proceedings 26th European Photovoltaic Solar Energy Conference and Exhibiton, 2011, pp. 871–874.
[10] H. Fujiwara, M. Kondo, Effects of a-Si:H layer thicknesses on the performance of a-Si: h/c-si heterojunction solar cells, J. Appl. Phys. 101 (5) (2007) 054516.
[11] Z.C. Holman, A. Descoeudres, L. Barraud, F.Z. Fernandez, J.P. Seif, S.D. Wolf, C. Ballif, Current losses at the front of silicon heterojunction solar cells, IEEE J. Photovolt. 2 (1) (2012) 7–9.
[12] J. Haschke, O. Dupré, M. Boccard, C. Ballif, Silicon heterojunction solar cells: recent technological development and practical aspects - from lab to industry, Sol. Energy Mater. Sol. Cells 187 (2018) 140–153.
[13] L. Mazzarella, A.B. Morales-Vilches, L. Korte, R. Schlatmann, B. Stannowski, Ultra-thin nanocrystalline n-type silicon oxide front contact layers for rear-emitter silicon heterojunction solar cells, Sol. Energy Mater. Sol. Cells 179 (2018) 386–391.
[14] M. Bivour, S. Schröer, M. Hermle, Numerical analysis of electrical TCO/a-Si:H(p) contact properties for silicon heterojunction solar cells, Energy Proc. 38 (2013) 658–669.
[15] K.-U. Ritzau, M. Bivour, S. Schröer, H. Steinkemper, P. Reinecke, F. Wagner, M. Hermle, TCO work function related transport losses at the a-Si:H/tco-contact in SHJ solar cells, Sol. Energy Mater. Sol. Cells 131 (2014) 9–13.
[16] G. Nogay, J.P. Seif, Y. Riesen, A. Tomasi, Q. Jeangros, N. Wyrsch, F.J. Haug, S.D. Wolf, C. Ballif, Nanocrystalline silicon carrier collectors for silicon heterojunction solar cells and impact on low-temperature device characteristics, IEEE J. Photovolt. 6 (6) (2016) 1654.
[17] E. Kobayashi, N. Nakamura, K. Hashimoto, Y. Watabe, Rear-emitter silicon heterojunction solar cells with efficiencies above 22%, 28th European Photovoltaic Solar Energy Conference and Exhibition, 2013, 691-694.
[18] T. Watahiki, T. Furuhata, T. Matsuura, T. Shinagawa, Y. Shirayanagi, T. Morioka, T. Hayashida, Y. Yuda, S. Kano, Y. Sakai, H. Tokioka, Y. Kusakabe, H. Fuchigami,

Rear-emitter Si heterojunction solar cells with over 23% efficiency, Appl. Phys. Express 8 (2) (2015) 021402.
[19] M. Bivour, H. Steinkemper, J. Jeurink, S. Schröer, M. Hermle, Rear emitter silicon heterojunction solar cells: fewer restrictions on the optoelectrical properties of front side TCOs, Energy Proc. 55 (2014) 229–234.
[20] S. De Wolf, C. Ballif, M. Kondo, Kinetics ofa-Si:H bulk defect anda-Si: h/c-si interface-state reduction, Phys. Rev. B 85 (11) (2012).
[21] R.A. Street, Localized states in doped amorphous silicon, J. Non-Cryst. Solids (1985) 1–16 (77 and 78).
[22] J. Cho, D.P. Pham, J. Jung, C. Shin, J. Park, S. Kim, A.H. Tuan Le, H. Park, S.M. Iftiquar, J. Yi, Improvement of hydrogenated amorphous silicon germanium thin film solar cells by different p-type contact layer, Mater. Sci. Semicond. Process. 41 (2016) 480–484.
[23] D.P. Pham, S. Kim, A.H. Tuan Le, J. Park, J. Yi, Diminished band discontinuity at the p/i interface of narrow-gap a-SiGe:H solar cell by hydrogenated amorphous silicon oxide buffer layer, J. Alloy. Compd. 762 (2018) 616–620.
[24] A. B. Morales-Vilches, L. Mazzarella, M. Hendrichs, L. Korte, R. Schlatmann, B. Stannowski, Nanocrystalline vs. amorphous n-type silicon front surface field layers in silicon heterojunction solar cells: role of thickness and oxygen content, 33rd European Photovoltaic Solar Energy Conference and Exhibition, 2017, 715.
[25] L. Mazzarella, A.B. Morales-Vilches, M. Hendrichs, S. Kirner, L. Korte, R. Schlatmann, B. Stannowski, nanocrystalline n-type silicon oxide front contacts for silicon heterojunction solar cells: photocurrent enhancement on planar and textured substrates, IEEE J. Photovolt. 8 (1) (2018) 70–78.
[26] C. Shin, S.M. Iftiquar, J. Park, S. Ahn, S. Kim, J. Jung, S. Bong, J. Yi, Radio frequency plasma deposited boron doped high conductivity p-type nano crystalline silicon oxide thin film for solar cell window layer, Mater. Chem. Phys. 159 (2015) 64–70.
[27] T. Roschek, T. Repmann, J. Müller, B. Rech, H. Wagner, Comprehensive study of microcrystalline silicon solar cells deposited at high rate using 13.56 MHz plasma-enhanced chemical vapor deposition, J. Vac. Sci. Technol. A: Vac. Surf. Films 20 (2) (2002) 492–498.
[28] O. Vetterl, F. Finger, R. Carius, P. Hapke, L. Houben, O. Kluth, A. Lambertz, A. Muck, B. Rech, H. Wagner, Intrinsic microcrystalline silicon: a new material for photovoltaics, Sol. Energy Mater. Sol. Cells 62 (2000) 97–108.
[29] E. Vallat-Sauvain, U. Kroll, J. Meier, A. Shah, J. Pohl, Evolution of the microstructure in microcrystalline silicon prepared by very high frequency glow-discharge using hydrogen dilution, J. Appl. Phys. 87 (6) (2000) 3137–3142.
[30] J. Koh, A.S. Ferlauto, P.I. Rovira, C.R. Wronski, R.W. Collins, Evolutionary phase diagrams for plasma-enhanced chemical vapor deposition of silicon thin films from hydrogen-diluted silane, Appl. Phys. Lett. 75 (15) (1999) 2286–2288.
[31] A.S. Ferlauto, R.J. Koval, C.R. Wronski, R.W. Collins, Extended phase diagrams for guiding plasma-enhanced chemical vapor deposition of silicon thin films for photovoltaics applications, Appl. Phys. Lett. 80 (15) (2002) 2666–2668.
[32] S.W. Kwon, J. Kwak, S.Y. Myong, K.S. Lim, Characterization of the protocrystalline silicon multilayer, J. Non-Cryst. Solids 352 (9–20) (2006) 1134–1137.
[33] L. Mazzarella, S. Kirner, O. Gabriel, S.S. Schmidt, L. Korte, B. Stannowski, B. Rech, R. Schlatmann, Nanocrystalline silicon emitter optimization for Si-HJ solar cells: substrate selectivity and CO2 plasma treatment effect, Phys. Status Solidi (a) 214 (2) (2017) 1532958.
[34] S.S. Hegedus, Current voltage analysis of a-Si and a-SiGe solar cell including voltage dependent photocurrent collection, Prog. Photovolt. Res. Appl. 5 (1997) 151–168.
[35] D.P. Pham, S. Kim, J. Park, J. Cho, H. Kim, A.H.T. Le, J. Yi, Role of a-Si:H buffer layer at the p/i interface and band gap profiling of the absorption layer on enhancing cell parameters in hydrogenated amorphous silicon germanium solar cells, Optik 136 (2017) 507–512.
[36] D.P. Pham, S. Kim, J. Park, A.H.T. Le, J. Cho, J. Yi, Improvement in carrier collection at the i/n interface of graded narrow-gap hydrogenated amorphous silicon germanium solar cells, J. Alloy. Compd. 724 (2017) 400–405.
[37] A. Lambertz, V. Smirnov, T. Merdzhanove, K. Ding, S. Haas, G. Jost, R.E.I. Schropp, F. Finger, U. Rau, Microcrystalline silicon-oxegen alloys for application in silicon solar cells and modules, Sol. Energy Mater. Sol. Cells 119 (2013) 134–143.
[38] P. Cuony, D.T.L. Alexander, I. Perez-Wurfl, M. Despeisse, G. Bugnon, M. Boccard, T. Soderstrom, A. Hessler-Wyser, C. Hebert, C. Ballif, Silicon filaments in silicon oxide for next-generation photovoltaics, Adv. Mater. 24 (2012) 1182–1186.
[39] S.M. Iftiquar, The roles of deposition pressure and rf power in opto-electronic properties of a-SiO:H films, J. Phys. D Appl. Phys. 31 (1998) 1630–1641.